Optimal wind-solar energy mix in Italy: Impact of climate variability

Alexis Tantet, Stéfanon Marc, Philippe Drobinski, Jordi Badosa, Concettini Silvia, Anna Creti, Claudia d'Ambrosio, Thomopulos Dimitri, Tankov Peter

Optimal wind-solar energy mix in Italy: Impact of climate variability

Tantet A.[a,*], Stéfanon M.[a], Drobinski P.[a], Badosa J.[a], Concettini S.[b,c], Creti A.[c,d], D'Ambrosio C.[e], Thomopulos D.[e], Tankov P.[f]

[a] *LMD/IPSL, École polytechnique, Sorbonne Université, ENS, PSL University, CNRS, Palaiseau, France*
[b] *IRJI, Université de Tours, Tours, France*
[c] *Département d'Economie, École polytechnique, Palaiseau, France*
[d] *Université Paris Dauphine, PSL, Leda-CGEMP, Paris, France*
[e] *LIX, École polytechnique, CNRS, Palaiseau, France*
[f] *CREST, ENSAE, École polytechnique, Palaiseau, France*

Abstract

In the context of the 2009 EU directive promoting the use of energy from renewable sources, Italy has reached its 2020 target of a 17% share of renewables in the final energy consumption 6 years in advance. In this study, we evaluate the existing renewable energy mix in Italy at regional scale by comparing it to an optimized mix taking into account climate variability and allowing full decommissioning of the currently installed plants. The variability of the production and of the demand over the 1989–2012 period is resolved by plugging regional climate simulations of this period into a model simulating the renewable energy production as well as the Italian electrical consumption at regional scale. The optimal mix is then inferred from a mean-risk analysis with as objectives both to maximize the mean of the total renewable production and to minimize the variance, or risk, of the latter. We consider two cases: in the first one the analysis takes cross-region correlations in the production and the demand into account and in the second one the analysis is local to each region. The optimal mix maximizing the ratio of the total mean penetration over the total risk for the same renewable capacity as installed in 2015 consists of about two thirds wind and one third solar, i.e. twice as much wind as the actual 2015 Italian renewable mix. The spatial distribution also differs significantly from the actual mix and from what would be obtained ignoring the risk and low-frequency climate variability.

Keywords: Energy, Renewable, Climate, Variability, Mediterranean

*,Corresponding author (alexis.tantet@lmd.polytechnique.fr)

Highlights

- Taking into account the risk strongly impacts the optimal Italian renewable mix.
- The risk should account for climate variability from hours to decades.
- The actual Italian mix could yield a higher renewable penetration at a lower risk level after geographical optimization.

1. Introduction

The world net electricity generation is expected to increase by 45% between 2015 and 2040 (IEA, 2017). In view of climate change and energy security concerns, the renewable energies will inevitably play a major role in satisfying this growing demand. Non-hydropower Renewable Energy Sources (RES) are the fastest-growing energy sources for new generation capacity and their share is expected to grow from 7% of total world generation in 2015 to 15% in 2040, with more than half of this growth coming from the wind power (IEA, 2017).

However given the variable nature of the RES production and the need for a constant supply-demand balance, increasing penetration of renewables raises structural, technological and economical issues. On one hand, variability may lead to local power shortages or increased transmission congestion. This must be compensated at all times by an increased flexibility of the conventional generation systems such as coal plants or combined cycle gas turbines (Huber et al., 2014). On the other hand, it brings higher price instability along with a reduction of the wholesale prices. In the long run falling prices may 'erode' the returns of both renewable and conventional producers, eventually pushing the latter out of the market while they are essential to smooth out the fluctuations of renewable power output and ensure system stability. Thereby the possibilities for a future large-scale renewable capacity are limited (Hirth, 2013; Spiecker and Weber, 2014).

Technological and spatial diversification are possible strategies to circumvent the problem of intermittency. In Europe, wind and solar-generated electricity roughly have negatively correlated seasonal cycles, solar generation being maximal in summer and wind generation in winter (Heide et al.,

2010). Spatial diversification is only applicable at large scale, whenever the RES variability is sufficient (see Widén (2011) for a study focusing on Sweden and Tsuchiya (2012) analyzing Japan). In light of those considerations, questions can be asked about how to implement this double strategy of diversification.

Technological and geographical optimization of renewable energy systems within a multi-objective framework has been discussed by several authors at continent and country scales. Complete electrical systems have been designed to quantify the requirements in installed power, transmission grid and storage capacity for a 100% of renewable energy scenario over Europe. For example, at the European scale, Heide et al. (2011) optimize the wind/solar mix in a fully renewable future European power system to reduce the storage and balancing needs; Rodríguez et al. (2014) do the same for the cross-border transmission capacities in the future; and Becker et al. (2014b) investigate the change in the optimal wind/solar mix in Europe as the transmission grid is enhanced. Becker et al. (2014a) optimize the wind/solar mix in the US to reduce storage needs and Nelson et al. (2012) simulate how a range of generation technologies, storage and transmission may meet the projected energy demand in the US at the least societal cost. Finally, Elliston et al. (2012) analyze how the Australian renewable mix should change in order to reduce the need for backup generation; and Lund and Mathiesen (2009) discuss feasible energy mix scenarios for a fully renewable electricity supply in Denmark.

Other conceptual frameworks with less ambitious energy targets have been explored at continental and regional scale by repowering the current installed renewable energy capacity. Repowering consists in fully decommissioning current renewable energy capacity and in re-allocating this capacity according to specific objectives (Del Río et al., 2011). For example, Beltran (2009) applies the mean-variance optimization techniques to infer the optimal energy mix; Roques et al. (2010) use similar methods to determine optimal wind power deployment among 5 European countries; Thomaidis et al. (2016) and Santos-Alamillos et al. (2017) use mean-variance optimization to assess the optimal wind and solar deployment and repowering actions in Spain. These studies use the Markovitz mean-variance portfolio theory or analogous methodologies to define the optimal full re-allocation of existing power plants among regions. It relies on a trade-off between maximizing the mean renewable productivity while minimizing the aggregate renewable energy supply risk (i.e. variability).

The majority of assessments of the optimal renewable energy mix are based on the statistical properties of the historical production and demand. Due to the only recent deployment of wind and solar energy systems the length of regional production and demand time series is often limited to a few years, which is not sufficient to properly take into account the effect of multi-annual climate non-stationarity at time scales of the life cycle of a wind and solar farm ($\sim 30y$) and reliably estimate statistics such as the mean and the covariance of the production.

In this article, we develop a methodology to analyze the repowering strategies of wind and solar plants in Italy and evaluate the current renewable mix. We determine the optimal geographical distribution of each renewable energy source using a mean-variance optimization. In addition to focusing on a different region than the aforementioned studies, our work presents the following important methodological novelty. Models of electricity generation and consumption are designed to feature climate variables such as the wind speed, the solar irradiance and the temperature. These variables are taken from a hindcast of the 1989–2012 period over the Mediterranean region (Fig. 1b). In this way, our mean-variance analysis — and additional statistical diagnostics such as the frequency of occurrence of shortage and saturation situations — takes into account the impact of interannual to intraday climate variability on the renewable production and the demand. Applying the model to Italy, we show that resolving such a large spectrum of time scales is essential to design a renewable energy system that remains optimal over its full life cycle. By replacing the hindcast simulations with future climate projections it is possible to use our methodology to study the impact of future climate evolutions including antropogenic climate change on the optimal renewable mix, however this is left for further research.

Italy offers an interesting case study of a market with high renewables penetration as it has reached its quota of 17% renewables in final energy consumption in 2014, therefore implementing the 2009 Climate Package six years ahead of the 2020 horizon (GSE, 2015). This is the result of ambitious support policies for RES development that have generated and still subsidize a significant amount of new investments, notably in solar and wind power plants.

The analysis of the Italian renewable mix is based on wind and solar photovoltaics (henceforth PV) production and electricity consumption computed from a regional climate simulation performed in the framework of two international programs — the Hydrological Cycle in the Mediterranean Ex-

periment (HyMex Drobinski et al., 2014) and the Coordinated Downscaling Experiment for the Mediterranean (Med-CORDEX Ruti et al., 2016). Two cases for the optimization of the renewable energy mix are investigated: in the first case, the Italian electrical network is considered as unique and the overall mix is optimized; in the second one, each interconnected zone minimizes its own risk in priority, ignoring potential benefits from taking covariance and interconnection between zones into account.

This article gives a first proof of concept that it is possible to design optimal renewable energy mixes taking into account climate variability over a large range of temporal scales. The remainder of the paper is structured as follows. Section 2 details the datasets, the simulation and the production and demand models on which is based the analysis of the optimal mix. The mean-variance optimization problem and its mathematical properties are presented in Section 3. In Section 4 we calculate the optimal geographical distribution of wind and solar generation in Italy and analyze the properties of these mixes in terms of weight given to each technology and in terms of occurrence frequency of shortage and saturation situations. The impact of climate variability on the optimal mixes is discussed in Section 5, together with their comparison with the actual wind-solar mix in Italy. In Section 6 we draw conclusions. The robustness of the numerical results to the climate data, the sampling and the model is tested in SI-1.

2. Data

2.1. GME and GSE databases

Time series of the hourly Italian regional electricity demand and of the yearly regional renewable capacity factors are used to design the demand and generation models. These variables are extracted from two publicly available databases provided respectively by the market operator GME[1] and the energy operator GSE[2]. For this reason, we first briefly comment on the structure of the Italian electricity market and next describe the databases we use.

The Italian power market consists of 7 foreign virtual zones, 6 regional sub-markets, or bidding zones, and 5 poles of limited production. The 20

[1] Gestore del Mercato Elettrico: https://www.gse.it/dati-e-scenari/statistiche
[2]Gestore dei Servizi Energetici: https://www.gse.it/dati-e-scenari/statistiche

(a) Italian electrical regions.

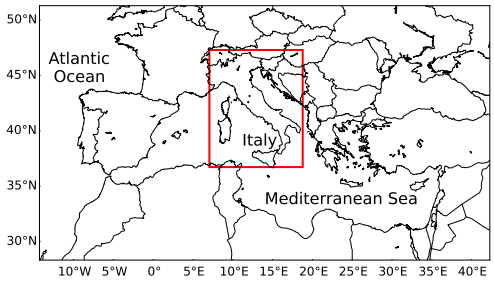

(b) Domain of the HyMeX/MED-CORDEX simulation covering Europe and the Mediterranean region. The rectangle indicates the domain of investigation of this study.

administrative regions composing the Italian territory are aggregated in the 6 bidding zones (Fig. 1a): Northern Italy (NORD), Central-Northern Italy (CNOR), Central-Southern Italy (CSUD), Southern Italy (SUD), Sardinia (SARD) and Sicily (SICI). Each zone has its own generation mix determined by historical and geographic reasons and characterized by a given level of efficiency. For instance, the Northern regions have larger hydroelectric production due to the proximity to the Alps. Inter-zonal transmission capacities are not equally distributed either.

The Italian power exchange, which is managed by the GME[3] is composed of a spot market, a forward market and a platform for the physical delivery of contracts concluded on the financial derivatives segment of the Italian Stock Exchange. The spot market is composed of three sub-markets: the day-ahead, the intraday and the ancillary services markets. We focus on the day-ahead submarket. The liquidity of the day-ahead market, calculated as the ratio of volumes traded on the day-ahead market to the total volumes (including bilateral contracts) of the Italian power system, has increased between 2010 to 2015, passing from 62.6% with 198 operators in 2010 to 67.8% with 259 operators in 2015. The peak liquidity has been reached in 2013 with a 71.6% liquidity and 214 operators (GME, 2017).

The GME database encompasses hourly bids and offers in the wholesale

[3] The GME manage as well the OTC Registration Platform for forward electricity contracts that have been concluded off the bidding system.

electricity market from 2004 to 2017; the offers are identified by supplier's technology. The hourly electricity demand is appraised from this source. GSE annual reports (e.g. GSE, 2016) contain information about the yearly electrical production and the associated installed capacity[4] detailed by region and sources from the beginning of 2008 to the end of 2016. At the beginning of this period, the installation of renewable energy capacity has shown a very rapid increase.

The regional time-mean capacity factors for PV and wind are calculated from this source. Since 2013, the PV and wind capacity factors are relatively stable. The demand and the capacity factors for PV and wind for the 2013–2017 period are presented in Table 1.

Region	Electrical demand (GWh/day — %)	Capacity Factor (PV — Wind)
NORD	312.2 — 56.5	12.1 — 20.4
CNOR	50.4 — 9.1	13.3 — 19.2
CSUD	82.0 — 14.9	14.1 — 18.8
SUD	44.2 — 8.0	15.6 — 20.9
SARD	26.7 — 4.8	14.5 — 19.6
SICI	36.8 — 6.7	15.9 — 18.7

Table 1: Regional electrical demand (from GME) and capacity factors for PV (blue) and wind energy (green, both from GSE) averaged over the 2013–2017 period.

Table 2 summarizes the regional information on electrical installation — in particular the current installed capacity and transmission lines — at the end of 2015. In addition, Figure 2 represents the geographical distribution of the installed RES capacity. The PV (wind) installed capacity is 18.8 GW (8.9 GW). The Northern cross-border region contains the majority of the phovoltaic plants as well as the power lines. The Southern region has most of the Italian wind turbines and has the second transmission capacity, to foreign markets. Note that the electricity demand to Italy from other countries is not taken into account in this study. The share of the renewable energy production in the electricity demand over the six regions in 2015 is found to be 19.4%.

[4]In the GSE reports, the capacity for a particular year is the installed capacity at the end of this year.

Region	Transmission lines (MW)	PV installed capacity (MW)	Wind energy installed capacity (MW)
NORD	53400	8241	113
CNOR	4550	2256	133
CSUD	12720	2631	1582
SUD	34100	3600	4351
SARD	595	721	1001
SICI	10100	1302	1753

Table 2: Characteristic of regional electrical infrastructure based on GSE database.

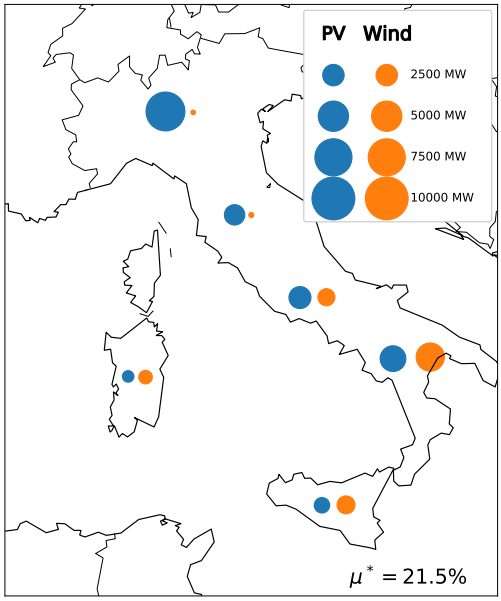

Figure 2: Geographical and technological distribution of the RES capacity installed by the end of 2015 in Italy (GSE database).

2.2. Regional climate simulations

A third variable employed in our study is the multi-year series of RES production. The deployment of RES capacity being relatively recent (starting around 2008 in Italy), available time series of observed RES production are not sufficiently long to estimate statistics taking into account low-frequency climate variability. To take into account climate variability, RES production is instead computed using regional climate simulations covering the historical

1989 to 2012 period.

We use the version 3.1.1 of the Weather Research and Forecasting Model (WRF). WRF is a limited area model, non-hydrostatic, with terrain following eta-coordinate mesoscale modeling system designed to serve both operational forecasting and atmospheric research needs (Skamarock et al., 2005). The WRF simulation has been performed in the framework of HyMeX and MED-CORDEX programs with a 20 km horizontal resolution over the domain shown in Fig. 1b between 1989 and 2012 with initial and boundary conditions provided by the ERA-interim reanalysis and updated every 6 hr (Dee et al., 2011). The WRF simulation has been relaxed towards the ERA-I large scale fields (wind, temperature and humidity) with a nudging time of 6 hr (Salameh et al., 2010; Omrani et al., 2013, 2015). A detailed description of the simulation configuration can be found in e.g. Flaounas et al. (2013).

The simulation has been evaluated against ECA&D gridded precipitation and precipitation at the Mediterranean basin scale (Flaounas et al., 2013), and have been used to study heatwaves (Stéfanon et al., 2014; Chiriaco et al., 2014), heavy precipitation (Lebeaupin Brossier et al., 2013, 2015; Berthou et al., 2014, 2015, 2016) and offshore wind energy potential assessment (Omrani et al., 2017) in a configuration coupled or not with a regional ocean model for the Mediterranean Sea (Drobinski et al., 2012). The simulation is available on the HyMex/MED-CORDEX database[5].

In the following sections, we describe the models used to estimate the wind and solar production and the electricity demand from the daily climate data. A large fraction of the variance of the production and of the demand is contained in shorter periods than a day and significantly impact the results of the mean-variance analysis (see SI-1). The production and demand models thus all include a parameterization of the intraday variability.

2.2.1. Electricity production model

To compute wind energy production simulated daily-mean horizontal wind-speeds are interpolated at hub height (101 m) using an empirical power-law with exponent 1/7 (Justus and Mikhail, 1976). A transfer function based on the power curve of a particular wind turbine, the relatively representative Siemens SWT-2.3 MW-101m, is applied to the wind speed to compute the

[5] `ftp://www.medcordex.eu/MED-18/IPSL/ECMWF-ERAINT/evaluation/r1i1p1/IPSL-WRF311/v1/day/`

electrical production at each climate-data gridpoint (Omrani et al., 2017)[6] Before applying the transfer function, the wind speed at hub height is multiplied by a factor $(\rho/\rho_0)^{(1/3)}$ accounting for deviations of the daily-mean air density ρ from the standard density ρ_0 for which the power curve has been obtained. The air density ρ is computed from the air temperature, pressure, and specific humidity at the surface from the WRF dataset using the ideal gas law for moist air[7].

In addition, it is essential in the mean-variance analysis to take intraday fluctuations of the wind production into account. In order to take into account intraday wind fluctuations in the variance of the wind capacity factors, hourly realizations of the wind speed to be fed to the transfer function are obtained by randomly drawing samples from a Rayleigh distribution with mean given by the daily-mean speed at hub height. In other words, the wind magnitude $V(d,h)$ at day d and hour h at some gridpoint is drawn from the Rayleigh distribution

$$f(x|\sigma(d)) = \frac{x}{\sigma^2(d)} e^{-\frac{x^2}{2\sigma^2(d)}}, \quad x \geq 0 \tag{1}$$

$$\text{with} \quad \sigma(d) = \sqrt{\frac{2}{\pi}}\overline{V}(d), \tag{2}$$

where the mode $\sigma(d)$ is defined such that the mean of the Rayleigh distribution is equal to the available daily-mean wind-speed $\overline{V}(d)$ at the gridpoint. The effect of this parameterization of intraday wind fluctuations on the wind capacity factor of the north region is shown in Figure 3a and 3b, for a sample week in winter and another in summer 2010, respectively. One can see how the capacity factor increases with the daily-mean wind-speed, as well as the variance of intraday fluctuations due to the parameterization. However, it is clear from the figure that the intraday variability of the capacity factor is underestimated, a discrepancy that should be improved in future versions of the model.

[6] Note that, due to the bias correction (see Sect. 2.2.2), only the variability of the wind production may be sensitive to this choice of power curve.

[7] This correction is applied to the wind speed rather than directly to the wind production in order to shift the power curve horizontally rather than scale it vertically and hence preserve the cut-in and cut-out behavior of the turbine.

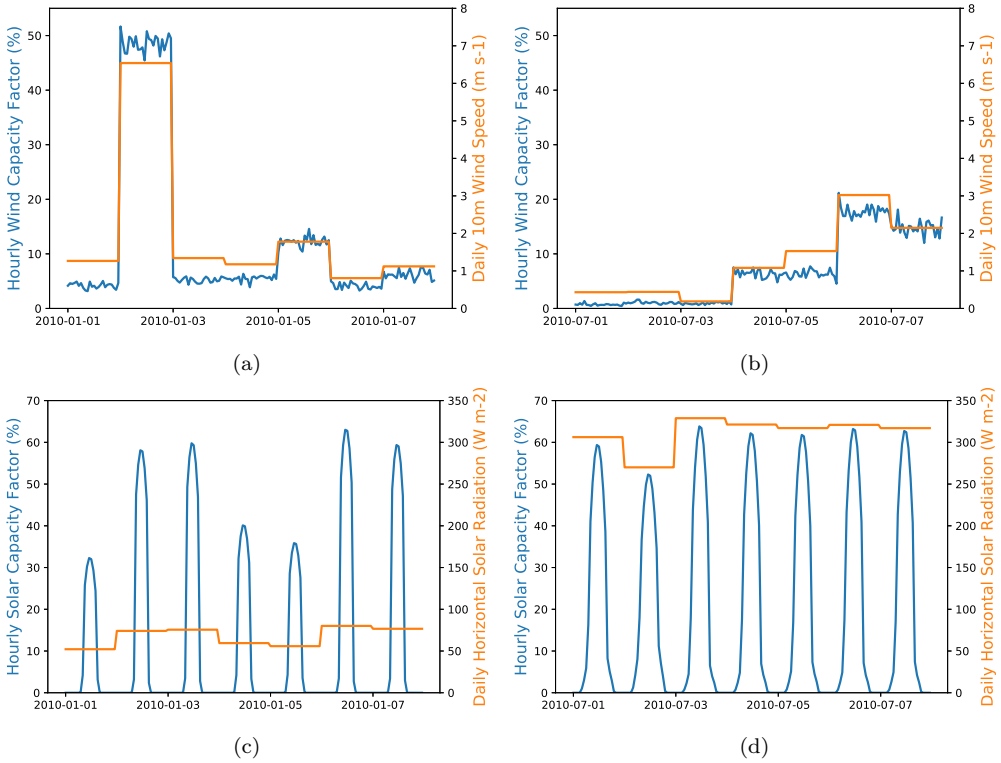

Figure 3: Illustration of the intraday parameterization of the wind (top) and solar (bottom) generation for the north region, the first week of January 2010 (left) and of July 2010 (right). Top panels represents both the computed hourly wind capacity factor (blue) and the daily-mean wind-speed (orange) from which the former is calculated. Bottom panels represents both the computed hourly solar capacity factor (blue) and the daily-mean horizontal surface radiation (orange) from which the former is calculated.

We simulate the PV production for arrays at each gridpoint composed of multi-crystalline silicon solar cells. The crystalline silicon solar cell occupies about 90% of the PV market, among which multi-crystalline solar cells have the highest share at 53% and mono-crystalline solar cells have a 33% share (Hosenuzzaman et al., 2015). Each module has a nominal power of $250\,\mathrm{Wm}^{-2}$ for an area of $1.675\,\mathrm{m}^2$, resulting in a reference efficiency of about 15%[8]. The real efficiency of the cell is, however, dependent on its temperature, which is itself dependent on the air temperature and the wind from the

[8]The nominal power itself is not important here, as only capacity factors are used

WRF dataset and on the global tilted irradiance (see below). This dependence is modeled using the thermal model described in Duffie and Beckman (2013, Chap. 23)[9]. The efficiency of the overall electrical installation behind the modules is assumed to be of 86%.

Solar radiation from WRF is partitioned into direct, diffuse and reflected components (Duffie and Beckman, 2013, Chap. 2.16) at every gridpoint. This partitioning depends on the clearness index $\bar{K}_T$ and elevation angle of the sun at the gridpoint. The quantity $\overline{K}_T(d)$, for some day d, is defined as the ratio of the horizontal radiation at ground level, $\overline{I}(d)$, to the corresponding radiation available at the top of the atmosphere, i.e. the extraterrestrial radiation $\overline{I}_0(d)$.

In order to take into account the effect of the diurnal cycle on the tilted irradiance, which accounts for most of the variance of the solar production (see Sect. SI-1), the hourly extraterrestrial solar radiation, $I_0(d,h)$, is computed for every hour h from the calendar information. The hourly horizontal radiation at the surface, $I(d,h)$, for the hour h of the day d is then computed by multiplying the hourly extraterrestrial radiation $I_0(d,h)$ by the clearness index $\overline{K}_T(d)$, assumed constant throughout the day. In other words,

$$I(d,h) = \overline{K}_T(d)\ I_0(d,h) \tag{3}$$

$$\text{with} \quad \overline{K}_T(d) = \frac{\overline{I}(d)}{\overline{I}_0(d)}. \tag{4}$$

Each array is assumed to be tilted by an angle equal to the latitude of the array and to face due South. To separate the diffuse component from the direct component of the global horizontal irradiance, the model from Reindl et al. (1990a) is used. For solar elevations below 10° and when the sun is behind the array, the direct horizontal irradiance is set to zero. The diffuse component of the tilted irradiance is computed following the model of Reindl et al. (1990b). The reflected component of the tilted irradiance depends on the zenith angle and follows the usual formula given by Duffie and Beckman (2013, Chap. 2.16) with an albedo of 0.2[10].

[9] The thermal model is configured for relatively common parameter values for cristalline cells, i.e., for a temperature coefficient of $0.004\,\mathrm{K}^{-1}$, a reference temperature of 25 °C and a cell temperature at nominal operating cell temperature of 46 °C (Skoplaki and Palyvos, 2009).

[10] The global tilted irradiance tends, however, to be dominated by its direct and diffuse

The effect of the diurnal cycle on the solar capacity factor of the north region is shown in Figure 3c and 3d, for a sample week in winter and another in summer 2010, respectively. One can see how the solar production varies with the diurnal cycle and how this cycle is modulated by the clearness of the atmosphere. On the other hand, no variability associated with intraday changes in, e.g., the cloud cover is present since the clearness index remains fixed throughout the day. The variance of the solar capacity factor may thus be underestimated. This discrepancy should, however, remain limited to the extent that intraday variations of the clearness index are averaged out by the regional averages.

2.2.2. Aggregation and bias correction

The regional wind and PV capacity factors are obtained by dividing the computed production by its nominal value and then aggregating at regional level on an hourly basis. In so doing, a strong bias (up to 100%) is found between the yearly-averages of the computed capacity factors and the region's capacity factors computed from the GSE data (Table 1). Since the second moment of the capacity factors roughly scales with their mean, we re-scale the computed capacity factors so that their average over the climate-data period (1989–2012) coincide with the GSE averages over the 2013–2017 period.

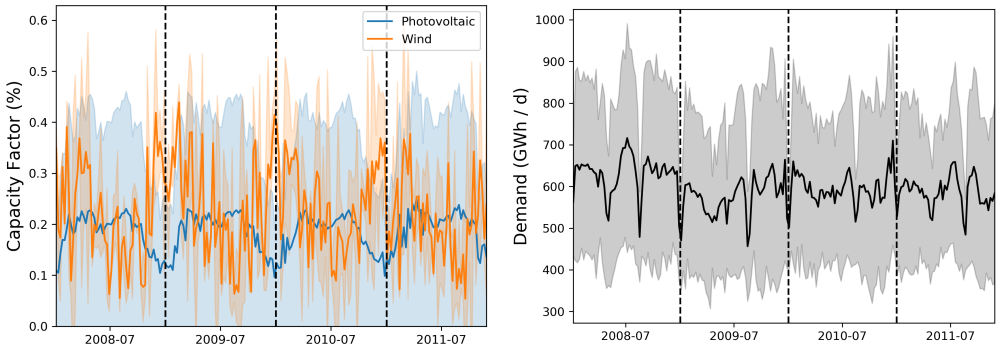

(a) (b)

Figure 4: Time evolution of weekly-averaged PV (orange) and wind (blue) capacity factors (a) and demand (b). The shadings represent the standard deviation of the time series.

components.

Figure 4a represents the weekly and regionally-averaged PV (orange) and wind (blue) capacity factors for a few sample years. Seasonal cycles of PV and wind energy production are phase shifted, with wind energy production (PV) peak yield in winter (summer). Wind energy production is also characterized by a stronger sub-seasonal variability when compared to PV at large-scale. Both the mean and the variance of the capacity factors for the wind production tend to be larger than those of the photovoltaic production. Albeit complementary over the year the wind and solar production requires additional energy inputs from other sources to counterbalance some recurrent short term deficit between the demand and the wind and solar production.

Let us insist that the present bias correction only corrects for differences in the first moment of the capacity factors with the observed values. For the analysis of Section 4, higher moments, in particular the variance and covariance, are also important. Although one expects the variance of the capacity factors to scale with their mean, discrepancies may persist. Our computations are tested against observations for bias in the variance in the SI-1.

Note finally that the conventional production, which includes here thermal as well as hydropower plants, is not explicitly modeled in this study and is left for future work.

2.2.3. Electricity demand model

Since we are primarily interested in the impact of climate variability and change on the demand, the objective of the model is to predict the part of the daily regional demand depending on climate, in particular on the surface air temperature[11], while preserving the statistics associated with other factors.

We follow a statistical learning approach (Hastie et al., 2009) whereby the model is trained against the regionally-averaged temperature data from the WRF model as input and the regionally-averaged demand data from GME as output, from the beginning of 2005 to the end of 2011 (i.e. the intersection of the climate with the demand record).

Let the electricity demand D_{in} for the region i at the time step n and for a particular type of day (see below) be given by

$$D_{in}(T_i) = f_i(T_{in}) + \epsilon_{in}. \tag{5}$$

[11] Other variables, such as the specific humidity, the wind, or the irradiance where not found to significantly affect the demand, in this case.

where $f_i, 1 \leq i \leq N$ is some real-valued function of the daily-mean temperature T_{in} in the region i at the time step n (T_{in} is the same for two hours of the same day), and the residual ϵ accounts for other factors impacting the demand, such as changes in the population, the economy, tourism, individuals decisions, etc.

It is known that the demand has a nonlinear dependence on the temperature. Electric heating is switched on only for lower temperatures, while air conditioning is switched on only for higher temperatures. This can be seen in Figure 4b for Italy. The demand has two main peaks per year, one during winter and one during summer, and lows in spring and fall and during holidays. In winter, the consumption peak is due to heating, especially in the northern part of Italy (see below). In summer, the consumption peak is due to tourism and air conditioning (Terna, 2016). Figure 4 shows that, except for the summer period, wind energy production is well correlated with the demand, whereas PV production is negatively correlated with the latter.

Once an individual appliance is switched on, its electricity consumption is to a first approximation linear in the temperature. Assuming, that all consumers behave in the same way and that a consumer switches the heater (air conditioning) for a constant temperature threshold T_H (T_C), we define the functions f_i as a piecewise-linear function of the temperature. In addition, the behaviour of the consumers differs significantly for the week days, Saturdays, and Sundays and holidays (respectively marked *work*, *sat* and *off*, in the following) and the demand is known to strongly depend on the hour of the day (see SI-1). We thus choose to modulate the daily demand by a composite cycle which only depends on the hour of the day and the day type. The resulting model is given by,

$$f_i(T_{in}) = \begin{cases} f_i^{\text{work}}(T_{in}) & \text{if the day at } n \text{ is a working day} \\ f_i^{\text{sat}}(T_{in}) & \text{if the day at } n \text{ is a Saturday} \\ f_i^{\text{off}}(T_{in}) & \text{if the day at } n \text{ is a holiday,} \end{cases} \tag{6}$$

$$\begin{aligned} \text{with} \quad f_i^{\text{work|sat|off}}(T_{in}) &= a_H^{\text{work|sat|off}} \Theta(T_H - T_{in})(T_H - T_{in}) \;\; g_n^{\text{work|sat|off}} \\ &+ a_C^{\text{work|sat|off}} \Theta(T_{in} - T_C)(T_{in} - T_C) \;\; g_n^{\text{work|sat|off}} \\ &+ a_0^{\text{work|sat|off}} \;\; g_n^{\text{work|sat|off}} \end{aligned}$$

where Θ is the Heaviside step function[12] and the coefficients $g_n^{\text{work|sat|off}}$ are given by the average — over all days of the same day type and all hours of the same hour of the day — of the observed demand on which the model is trained. The model (6) has a total of 9 parameters $a_H^{\text{work|sat|off}}$, $a_C^{\text{work|sat|off}}$ and $a_0^{\text{work|sat|off}}$ to be adjusted, for each region.

The resulting linear model is fitted assuming that the thresholds T_H and T_C are constant over all regions and all day types. These thresholds constitute two hyper-parameters that we select via a grid-search with a cross-validation (Hastie et al., 2009) over seven blocks of one year.

The linear model is fitted using the Bayesian ridge regression method (MacKay, 1992) both to avoid over-fitting and to take into account the variance arising from factors that are not fully resolved by the deterministic part of the model[13]. A time series of the hourly regional demand over 1989–2012 is predicted from the full length of the temperature record by randomly drawing samples from the posterior distribution of the model at each time step. The way the Bayesian model operates is illustrated in Figure 5 where the predicted demand for the north region the first week of January 2010 is shown (plain blue line) together with the input daily-mean temperature T_{in} (plain orange line) and the series of composite daily cycles $g_n^{\text{work|sat|off}}$ (dashed blue line).

The resulting prediction of the regional demand is represented (only for daily-means) in Figure 6 versus the input temperature. The overall coefficient of determination is 0.73. One can see that the temperature and type of day dependence of the demand is most clear for the economically most dynamic north region. This is also true, yet to a lesser extent, for the central south region. The shaded regions show that the part of the demand that is not explained by the temperature model is compensated by the Bayesian perturbations, although in a random fashion.

To conclude, this method, as apposed to using the 13 years of observed demand provided by GME, allows to estimate the demand over the longer

[12] The relationship between the demand and the ambient temperature in European countries is smoother than a piecewise-linear function (Bessec and Fouquau, 2008), in part due to the non-homogeneous behaviour of the consumers. Here, however, we prefer to keep the model as simple as possible using the above linear basis.

[13] The implementation from *scikit-learn* (Buitinck et al., 2013) of the Bayesian ridge regression is used, whereby the residual and the weights are given zero-mean isotropic Gaussian priors. The variances of the latter are given as priors gamma distributions.

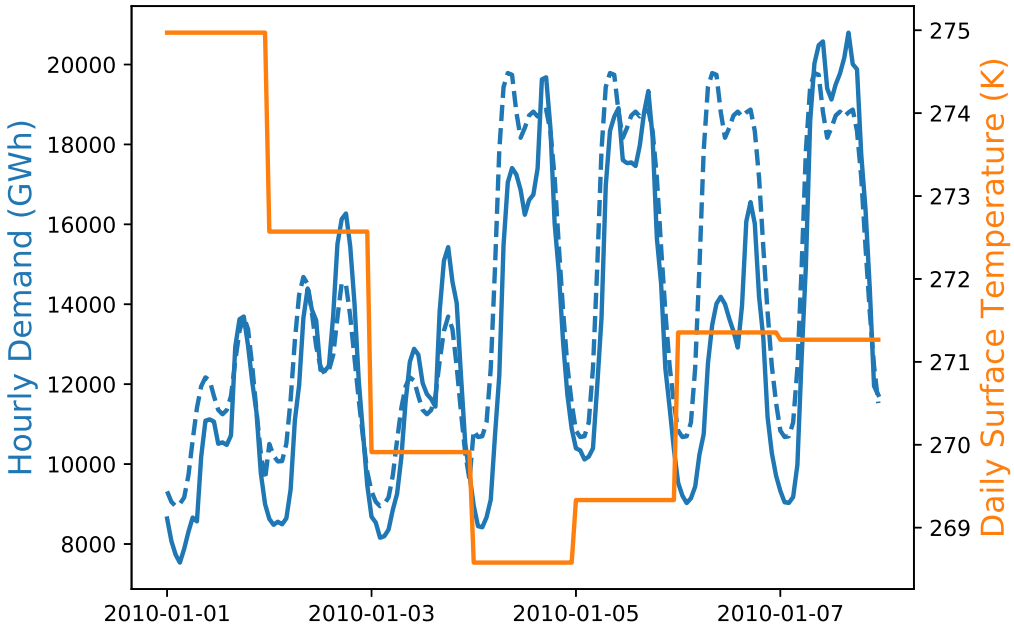

Figure 5: Illustration of the intraday parameterization of the demand for the north region the first week of January 2010. The computed hourly demand (plain blue line) is obtained by modulating the series of composite daily cycles $g_n^{\text{work|sat|off}}$ for each day type (dashed blue line) by the function (6) of the daily-mean temperature (plain orange line) and by adding random perturbations drawn from a normal distribution whose variance depends both on the noise in the demand and the uncertainty in the parameters of the model.

record of the climate data so as to take into account variations in the demand due to low-frequency temperature variability[14].

3. Mean-variance analysis

Geographic and technological diversification of renewable power plants is based on a mean-variance analysis that is inspired by Markowitz's modern portfolio theory[15].

[14]Note that, assuming that the demand-temperature relation in (6) is valid, low-frequency climate variability may be responsible in changes in the coefficients of the model over periods longer than the observed demand record over which the model is fitted.

[15] See, for example, Mencarelli and D'Ambrosio (2018) for a survey on mathematical programming approaches for the portfolio selection problem.

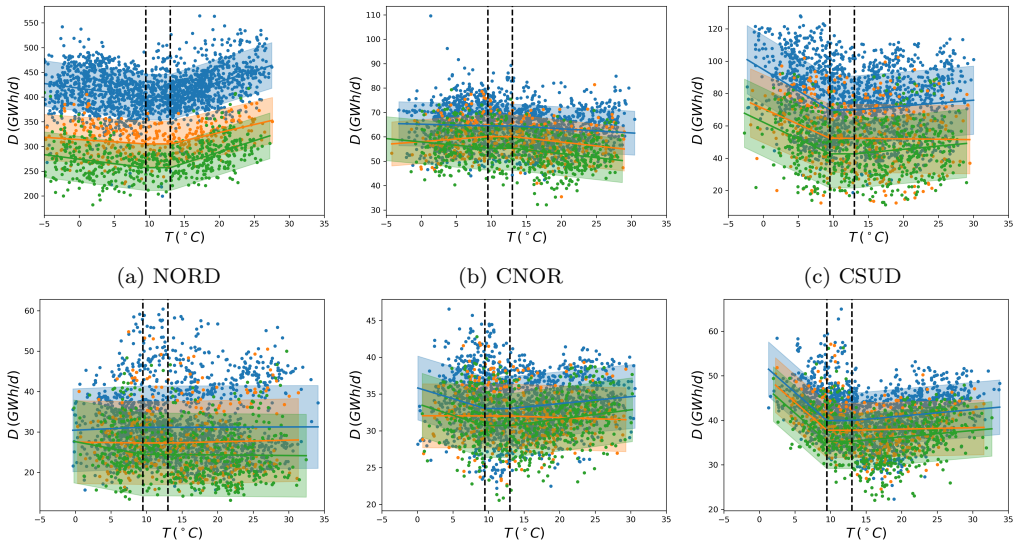

(a) NORD (b) CNOR (c) CSUD

(d) SUD (e) SARD (f) SICI

Figure 6: Daily-mean electricity demand for each zone versus the surface temperature. Each point is an observed realization of temperature and demand. The lines represent the functions $f_i^{\text{work|sat|off}}$ of the demand model, while the associated shaded regions represent the variance of the prediction. Blue, orange and green data points and functions correspond to working days, Saturdays, and Sundays and holidays, respectively. The two vertical dashed lines represent the temperature thresholds $T_H = 9.5$ and $T_C = 13.0$.

In our context, the mean-variance analysis refers to the process of finding optimal spatial and technological distributions of renewable energy production achieving a trade-off between the mean penetration rate and some measure of the variance in the renewable energy production. The variance is a proxy for the risk: minimizing the variance corresponds to maximizing the diversification of the renewable configuration, which in turn lowers the variability of renewable energy penetration and improves the flexibility of the system and its resistance to shocks. In particular, a lower variance in the renewable energy mix is less demanding in services from conventional production (for which start up and shutting down services have a cost) or demand management.

Each renewable mix may then be represented in a mean-variance chart. As a bi-objective optimization problem (Miettinen, 1999), mixes are to be optimal in the Pareto sense. A solution is said to be Pareto optimal if there exists no feasible solution with a better or equal value for each of the objective

functions (with at least one of these values being strictly better).

Let us consider as an example Figure 7. The points under or to the right of the frontier are by definition suboptimal and will be discarded by a rational investor. The area above or to the left of the frontier cannot be reached.

Two variations of the mean-variance analysis are considered here. In both, the mean RES penetration μ is given by the fraction of the expected total production over the expected total demand[16], i.e.

$$\mu := \frac{\mathbb{E}\left[\sum_{\mathbf{k}} w_{\mathbf{k}} \eta_{\mathbf{k}}\right]}{\mathbb{E}\left[\sum_i D_i\right]} = \frac{\sum_{\mathbf{k}} w_{\mathbf{k}} \mathbb{E}\left[\eta_{\mathbf{k}}\right]}{\mathbb{E}\left[\sum_i D_i\right]}, \tag{7}$$

where $\mathbf{k} = (i, j)$ is the multi-index composed of a regional index i in {NORD, CNOR, CSUD, SUD, SARD, SICI} and a technological index j in $\{\mathrm{PV}, \mathrm{wind}\}$, the $w_{\mathbf{k}}$ are the installed capacities for each region and technology, the $\eta_{\mathbf{k}}$ are the corresponding predicted time-dependent capacity factors (Sect. 2.2.1) and the D_i are the predicted regional demands (Sect. 2.2.3). Note that, in the following numerical applications, statistics such as the expectation or the covariance are replaced by sample estimates from the full records (1989–2012).

In the first strategy, also called *global*, it is assumed that each region produces electricity to satisfy the total demand in priority with no consideration for their local demand or for transmission constraints between regions. In other words, the electricity produced at a given location is immediately available to meet the overall Italian demand. In this case, the risk squared $\sigma^2_{\mathrm{global}}(\mathbf{w})$ is defined as the variance of the sum of the regional RES productions normalized by the total demand, i.e.

$$\sigma^2_{\mathrm{global}}(\mathbf{w}) := \mathbb{V}\left[\frac{\sum_{\mathbf{k}} w_{\mathbf{k}} \eta_{\mathbf{k}}}{\sum_i D_i}\right] = \sum_{\mathbf{k}} \sum_{\mathbf{l}} w_{\mathbf{k}} G^{\mathrm{global}}_{\mathbf{k},\mathbf{l}} w_{\mathbf{l}}, \tag{8}$$

where $G^{\mathrm{global}}_{\mathbf{k},\mathbf{l}} := \mathrm{Cov}[\eta_{\mathbf{k}} / \sum_i D_i, \eta_{\mathbf{l}} / \sum_i D_i]$ is the covariance matrix between the capacity factors normalized by the total demand for each pair of regions and technologies.

[16] The normalization by the mean total demand in the definition (7) of the mean penetration has no effect on the relative distribution of the capacities in the optimal problem.

In the second strategy, also called *regional*, each region attempts to satisfy its local demand in priority. If the electrical production is larger than the demand, electricity can be exported. The risk squared $\sigma^2_{\text{regional}}(\mathbf{w})$ is thus defined as the sum of the variances of the regional production normalized by the regional demand.

$$\begin{aligned}\sigma^2_{\text{regional}}(\mathbf{w}) &:= \sum_i \mathbb{V}\left[\frac{w_{(i,\text{PV})}\eta_{(i,\text{PV})} + w_{(i,\text{wind})}\eta_{(i,\text{wind})}}{ND_i}\right] \\ &= \sum_{\mathbf{k}}\sum_{\mathbf{l}} w_{\mathbf{k}} G^{\text{regional}}_{\mathbf{k},\mathbf{l}} w_{\mathbf{l}},\end{aligned} \tag{9}$$

where $G^{\text{regional}}_{\mathbf{k},\mathbf{l}} := \text{Cov}[\eta_{\mathbf{k}}/(ND_i), \eta_{\mathbf{l}}/(ND_j)]$ if $i = j$, 0 otherwise[17].

Note that in the global and the regional definitions of the risk, the RES production is normalized by the total and by the regional demand, respectively. This is particularly important for the regional optimization as normalizing by the local demand favors installing RES capacity in proportion to the latter.

The goal of this study being to assess the optimal recommissioning of the Italian renewable energy mix, we also consider constraining the total installed RES capacity to its observed value $w_{\text{total}} = 27.7\,\text{GW}$ in 2015 (Sect. 2.1). The mean-variance analysis, thus, consists in solving, the optimization problem

$$\begin{aligned}
&\min_{\mathbf{w}} && \sigma^2_{\text{global|regional}}(\mathbf{w}) && \text{(10a)}\\
&\max_{\mathbf{w}} && \sum_{\mathbf{k}} w_{\mathbf{k}}\mathbb{E}[\eta_{\mathbf{k}}] && \text{(10b)}\\
&\text{subject to} && \sum_{\mathbf{k}} w_{\mathbf{k}} = w_{\text{total}} && \text{(10c)}\\
& && w_{\mathbf{k}} \geq 0 \quad \forall\, \mathbf{k}. && \text{(10d)}
\end{aligned}$$

Assuming that the share of the demand that is not satisfied by RES is supplied by the conventional production normalized by the demand, the optimization problem (10) is equivalent to minimizing both the mean and the variance of the conventional production. Taking into account the full power

[17] The division by the number of regions N in (9) is there for comparison with the global risk (8).

flow of the transmission network together with the conventional production is left for future work.

The classical method used in the following Section 4 to approximate the optimal frontier numerically is explained in SI-2. In this study, we refer to the optimal frontier as the curve $\big(\sigma_{\text{global|regional}}(\hat{\mathbf{w}}), \mu_{\text{global|regional}}(\hat{\mathbf{w}})\big)$, where the $\hat{\mathbf{w}}$ are the optimal solutions, although, strictly speaking, it is the risk squared that is minimized rather than the risk itself. The numerical results of the following section suggest that the so-defined frontier of the bi-objective problem (10) without the total capacity constraint (10c) is a half line with a positive slope that we refer to as the *mean-risk ratio* $\alpha_{\text{global|regional}}$. In other words, the optimal mixes for this problem are such that

$$\mu_{\text{global|regional}}(\hat{\mathbf{w}}) = \alpha_{\text{global|regional}} \;\; \sigma_{\text{global|regional}}(\hat{\mathbf{w}}), \tag{11}$$

In the following, we assume that this is indeed the case and the mean-risk ratio $\alpha_{\text{global|regional}}$ is used to diagnose the variants of the optimization problem. The proof of a rigorous mathematical result is left for future work.

4. Optimizing the distribution of wind and solar generation

Global and *regional* strategies are represented in Figure 8 (upper and lower panels respectively). Each point of the frontier represents an optimal combination of the capacities that maximizes the penetration for a given risk, while satisfying the constraints. The mixes in the region below or to the right of the efficient frontier are suboptimal. The straight black line represents an approximation of the optimal frontier of the same problem, but with the total capacity constraint (10c) removed.

One may first observe that the optimal frontiers of the *regional* strategy (Fig. 8c) are shifted towards lower risk values compared to the frontiers of the *global* strategy (Fig. 8a). This shift is due to the different definitions (8) and (9) of the risk for the two strategies, respectively. It does not provide an objective argument to choose a regional policy over a global one. Instead, a trade-off exists between a strategy in which all regions cooperate for the national welfare and a strategy in which each region attempts to meet its own demand in priority[18].

[18] Recall from Sect. 3, that in this study, the constraints imposed by the conventional production and transmission network capacities are not considered.

The mean-risk ratio $\alpha_{\text{global|regional}}$ (the slope of the black curves) of the optimization problems without the total capacity constraint is also given in the sub-captions. It is of 1.69 for the *global* strategy and of 3.71 for the *regional* strategy. Increasing the mean penetration of the optimal mix necessarily comes at the price of an increased risk. For the same level of total mean penetration, adding the constraint on the present total capacity (blue curve) necessarily deteriorates the risk.

The point at which both frontiers join (in black) corresponds to the optimal mix for which the total capacity constraint is inactive. This means that, for this level of mean penetration, the mix minimizing the risk naturally satisfies the total capacity constraint. It is thus the optimal mix satisfying the total capacity constraint that has the maximum mean-risk ratio. If no preference is put on maximizing the mean penetration or minimizing the risk, this optimal mix is attractive. In the following, we refer to this mix as the *maximum mean-risk ratio scenario*.

Yet, one may be interested in allowing for the deterioration of the mean-risk ratio in order to either decrease the risk or increase the total penetration. The blue dots in Fig. 8a and 8c correspond to the optimal mixes minimizing the risk. Their mean-risk ratio is then lowered to a value of 1.61 for the global strategy and of 3.53 for the regional strategy. We refer to this mix as the *minimum risk scenario*. For comparison with the actual mix the blue diamond in Fig. 8a and 8c represents the optimal mix that satisfies the same level of risk as the actual mix (gray dot) while maximizing the penetration rate. We refer to this mix as the *high penetration scenario*.

Some important properties of the optimal mixes with the constraint on the total capacity are represented on the right panels of Fig. 8. The PV ratio, i.e. the fraction of photovoltaic capacity in the mix, is plotted in orange. A value of 100% (0%) corresponds to 100% (0%) PV production 0% (100%) wind energy production. The plain and dashed green curves represent the frequency of occurrence of shortage and saturation, respectively. Shortage situations are associated with insufficient energy production. This situation corresponds to large scale blocking atmospheric patterns associated with cold or heat waves and low renewable energy production, especially from wind. These configurations lead to underproduction of electricity from PV and wind farms. Here, it is assumed that conventional generation units are able to meet up to 80% of the maximum demand modeled. Shortage then occurs if the photovoltaic and wind generation is not able to meet the rest of the demand. In this case, electricity needs to be imported from the neighboring

countries (which is not explicitly accounted for in our modeling framework). Moreover, shortage situations result in an increase in the electricity market price and add pressure on power networks at continental scale. The second critical situation corresponds to network saturation, when electricity production from wind and PV plants is too large for the network and exceeds the technical limit of renewable energy fraction in the energy mix. In this study, saturation is defined to occur if more than 40% of the demand is met by photovoltaic and wind sources. High probability of occurrence of such situations may jeopardize the funding system for renewable energy infrastructures and may lead to network instability. It can also generate very low or even negative electricity prices (in Italy the prices cannot be negative, the floor is 0 euro), jeopardizing the profitability of the conventional power plants, which are essential for network security. Figures 8d and 8d show the fraction of installed PV capacity and the frequency of occurrence of shortage and saturation situations as a function of the mean penetration for the global and the regional strategy, respectively.

One can first see that the PV ratio is a decreasing function of the mean penetration reached by the mix. This is explained by the fact that the capacity factors from the wind generation are higher than those from the photovoltaic generation (cf. Tab. 1). Moreover, the shortage and the saturation curves (in green) have a distinct global minimum. The convexity of both curves is due to the fact that the probability of occurrence of extremes increases with the risk and that the latter increases faster for both smaller and larger values of the mean penetration. The vertical lines in Fig. 8b and 8d represent the level of mean penetration for the minimum risk, maximum mean-risk ratio and high penetration scenarios. The minimum risk, the maximum mean-risk ratio and the high penetration scenarios respectively include 45%, 33% and 19% of PV capacity in the mix. The minimum risk scenario is relatively close to the minimum of saturation occurrence, while the maximum mean-risk ratio and the higher penetration scenarios are close to the minimum of shortage occurrence. Thus, favoring the minimization of the risk also allows to avoid saturation situations, while increasing the mean penetration allows to avoid shortage situations. Overall, the regional problem suggests installing more photovolatic capacity than wind capacity compared to the global problem.

We represent in Figure 9 the resulting spatial distributions corresponding to the three scenarios for both the global and the regional problems. Focusing on the global problem, the minimum risk scenario distributes all

the PV capacity in the north region, while achieving higher levels of mean penetration requires to move the PV capacity to the south and to Sicily. For all scenarios, the wind capacity is relatively spread over all regions but the central south one.

The resulting capacity distribution for the regional strategy (right panels of Fig. 9) is dramatically different from that for the global strategy. Indeed, most of the RES capacity is installed in the north region, whatever the scenario, with more wind capacity to increase the mean penetration. Only minimal capacity is installed in the central north, Sardinia and Sicily. This can be understood from both facts that the definition of the risk for the regional problem favors minimizing the risk of each region individually before minimizing the total risk and that the capacity factors in the risk are normalized by the demand. Since most of the demand occurs in the north (cf. Table 1), the variance of the capacity factors in that region is given less weight than the others in the definition of the regional risk. This corresponds to an incentive for the north region to satisfy its demand with its own RES resource first.

The results obtained so far show a strong dependence of the optimal mix on the level of risk that should be achieved. A mix favoring a high level of mean production at the expense of the risk — like in the high penetration scenario — yields a very different PV ratio and geographical distribution of the renewable capacity than in mixes favoring a lower level of risk — like in the the maximum mean-risk ratio and minimum risk scenarios.

5. Discussion

The methodology developed in this article has specifically been designed (i) to exploit correlations between the RES production and the demand and between regions to optimize the renewable energy mix and (ii) to take into account the impact of the climate variability on this mix. This allows us to discuss in this section the role played by climate variability and the potential for improvement of the actual Italian mix.

5.1. Impact of climate variability on the mix

To assess the impact of interannual climate variability (as found in the CORDEX data) on the mix, we repeat the mean-variance analysis successively using data blocks of one year, from 1989 to 2010. In other words, the mix of the 22 mixes that we obtain is optimized for the climatic conditions of

a given year. As a result, the optimal mix for one year may be different from the optimal mix for another year due to low-frequency climate variability.

We focus on the mixes maximizing the mean-risk ratio α_{global} for the global strategy. From the 22 values of the mean-risk ratios associated with each year, we obtain an estimation of their mean value and of an interval containing 95% of their realizations (see SI-1 for more explanations). The mean-risk ratio α_{global} averages to 1.71 and 95% of its distribution belongs to the centered interval $[1.57, 1.85]$. Thus, even though the average of the yearly mean-risk ratio is close to the one of 1.69 obtained in Section 4 using the full record, interannual climate variability in the CORDEX data is responsible for year-to-year variations of the mean-risk ratio of up to 8.2%.

To go further, we represent in Figure 10 the geographical and technological distribution of the mixes for the year 1989, with a particularly low mean-risk ratio of 1.60, and for the year 1996, with a particularly high mean-risk ratio of 1.85. Due to the steeper optimal frontier for 1996, the mix for the maximum mean-risk ratio scenario achieves both a higher mean total penetration and a lower risk than that for 1989. The distribution of the RES capacity for 1996 also differs from that for 1989 as more wind capacity is installed in the central south and Sardinia regions.

It is thus clear that the low-frequency climate variability has a large impact on the optimal mix and that the latter should be taken into account in order to assess future optimal RES mixes that are robust to changes in the climate.

5.2. Comparison with the 2015 Italian mix

The 2015 (actual) Italian mix is composed of 68% PV and 32% wind energy capacity (see Table 2). As can be seen from Figure 2, the largest fraction of installed PV capacity is in the North of Italy, whereas most of wind capacity is located in the South. Indeed, Italy has started investing in renewable energy resources since 1991 (with the feed in tariff CIP6), with the objective of developing national energy sources and so decreasing the dependency on imported gas. Historically, the bulk of PV has been developed in Northern Italy, where the entrepreneurial background has favored local business exploiting renewable energy resources subsidies. Wind farms have been installed in Sicily and Sardinia, where regional specific incentives have been set. Southern Italy has invested in renewable energy more recently, after the reinforcement of the main North-South transmission line.

To compare the actual mix with the optimization results, the actual mean penetration and risk are computed for the actual capacity distribution using the same capacity factor and demand data as used to obtain the optimal frontiers of Fig. 8. The corresponding mix is represented by the gray dot in the same figure. This point is not visible in Fig. 8c, for the regional problem, because the value of its risk is several orders of magnitude larger than the x-axis limits. For both the global and the regional problem, the gray point is to the right of the optimal frontiers. The actual mix installed in Italy is thus sub-optimal. For the global problem, this mix reaches a level of mean penetration comparable to that of the minimum risk scenario, but its risk is about 29% larger than that of the latter and its PV ratio about 49% higher. The capacity distribution of the optimal mixes in Figure 9 may also be compared to that of the 2015 Italian mix in Figure 2. The actual mix appears to be closest to the minimum risk and maximum mean-risk ratio scenarios of the global problem (Fig. 9a). However, the actual mix favors photovoltaic over wind capacities, especially in the north, and that more RES capacity is installed in the central south region. This is in strong contrast with all optimal scenarios. For instance, the maximum mean-risk ratio scenario yields about two third (one third) of wind (solar) capacity. However, these differences may partly be attributable to biases in the intraday variance, as the model tends to underestimate intraday variance of the wind capacity factors and to overestimate the intraday variance of the solar capacity factors (see Table 1)[19].

6. Conclusion

This work is aimed at developing a proof-of-concept of an integrated modelling framework dedicated to the elaboration of optimal scenarios of renewable energy mix. The proposed framework relies on regional climate simulations. It is shown to be of practical interest for both short and long term renewable energy management, as the model is able to take into account variability in the renewable production and electricity demand from hourly to interannual time scales. The model allows to derive different scenarios consisting in either maximizing the total renewable energy penetration or

[19] Improving the resolution of the intraday variability of the production in the model may require to develop a better parameterization or to rely on additional data. This is left for future work.

minimizing the total risk by taking advantage of (anti-)correlations between regions and technologies in an optimal way. Different optimization strategies have been chosen to establish the renewable energy mixes: the first optimization strategy, the global one, maximizes the national Italian welfare by taking full advantage of correlations between region and by ignoring any potential network constraint; the second strategy, the regional one, assumes that each region maximizes its own welfare in priority, disregarding the potential benefit of exploiting cross-regional correlations to improve the national welfare.

The main results have been obtained by relying on the full length of the climate record (23 years), in order resolve the impact of interannual climate variability on the optimal mixes as well as possible. By computing additional mixes using only one year of climate data for all available years and by assessing the differences between these mixes, we could show that the impact of interannual climate variability on the optimal renewable energy mix should not be neglected.

Comparison with the actual Italian renewable energy mix shows that the actual mix is closer to the global strategy that to the regional strategy as the renewable capacity is relatively evenly spread among regions. However, the scenario maximizing the ratio of the total mean penetration over the risk yields about two thirds (one third) of wind (solar) capacity, in strong contrast with the actual mix containing one third of installed wind capacity. The reasons for such differences are difficult to identify as the actual renewable energy capacity deployment did not follow an optimization elaborated at country scale, but relied on regional policies. Conversely, our optimal energy mix scenarios rely on selected optimization strategies and may be prone to biases in the resolution of the intraday variance of the production.

The current framework takes the variance, or risk, of the fraction of the demand covered by the renewable production as a proxy for the flexibility service needed from the hydro and conventional production. Our modeling framework would benefit from the translation of this risk into an economic or a climate cost. For that purpose, the hydro and the conventional production would have to be modeled, taking into account reserve constraints and priority orders between these energy sources. The transmission network would also have to be modeled to take network constraints into account as well as the arbitrage between producing locally and importing/exporting between regions.

The current framework is also adapted to consider optimal strategies in a warming climate using 21st century projections from general circulation

models. Finally, the generalization of such integrated modeling tool at Euro-Mediterranean scale is a priority. Our framework opens the way for the study of energy transition scenarios at the European scale based on precise modeling of climate variability and climate change. The interconnected regions will then be replaced with interconnected countries.

7. Acknowledgments

AT is grateful to Mathilde Mougeot and Jérôme Collet for insightful discussions on modeling the electricity demand. This work was conducted in the framework of the TREND-X research program on energy transition at Ecole Polytechnique, which benefited from the support of the Ecole polytechnique fund raising – TREND-X Initiative. This research was also supported by the ANR project FOREWER (ANR-14-414 CE05- 0028) and the HyMeX project (HYdrological cycle in The Mediterranean EXperiment) through the working group Renewable Energy, funded by INSU-MISTRALS program. The TREND-X model is open-source and available on demand. The full documentation of the model is available at `https://www.lmd.polytechnique.fr/~atantet/TRENDX/`. It includes a reference guide and a tutorial, allowing one to easily reproduce the results of this study.

References

Becker, S., Frew, B. A., Andresen, G. B., Zeyer, T., Schramm, S., Greiner, M., Jacobson, M. Z., 2014a. Features of a fully renewable US electricity system: Optimized mixes of wind and solar PV and transmission grid extensions. Energy 72, 443–458.

Becker, S., Rodriguez, R. A., Andresen, G. B., Schramm, S., Greiner, M., 2014b. Transmission grid extensions during the build-up of a fully renewable pan-European electricity supply. Energy 64, 404–418.

Beltran, H., 2009. Modern Portfolio Theory Applied To Electricity Generation Planning. PhD Thesis, University of Illinois at Urbana-Champaign.

Berthou, S., Mailler, S., Drobinski, P., Arsouze, T., Bastin, S., Béranger, K., Flaounas, E., Brossier, C. L., Somot, S., Stéfanon, M., 2016. Influence of submonthly air–sea coupling on heavy precipitation events in the Western Mediterranean basin. Quarterly Journal of the Royal Meteorological Society 142 (S1), 453–471.

747 Berthou, S., Mailler, S., Drobinski, P., Arsouze, T., Bastin, S., Béranger,
748 K., Lebeaupin-Brossier, C., Dec. 2014. Prior history of Mistral and Tra-
749 montane winds modulates heavy precipitation events in southern France.
750 Tellus A: Dynamic Meteorology and Oceanography 66 (1), 24064.

751 Berthou, S., Mailler, S., Drobinski, P., Arsouze, T., Bastin, S., Béranger,
752 K., Lebeaupin-Brossier, C., 2015. Sensitivity of an intense rain event be-
753 tween atmosphere-only and atmosphere–ocean regional coupled models:
754 19 September 1996. Quarterly Journal of the Royal Meteorological Society
755 141 (686), 258–271.

756 Bessec, M., Fouquau, J., 2008. The non-linear link between electricity con-
757 sumption and temperature in Europe: A threshold panel approach. Energy
758 Econ. 30 (5), 2705–2721.

759 Buitinck, L., Louppe, G., Blondel, M., Pedregosa, F., Müller, A. C., Grisel,
760 O., Niculae, V., Prettenhofer, P., Gramfort, A., Grobler, J., Layton, R.,
761 Vanderplas, J., Joly, A., Holt, B., Varoquaux, G., 2013. API design for
762 machine learning software: experiences from the scikit-learn project. arXiv
763 1309.0238 [cs.LG], 15.

764 Chiriaco, M., Bastin, S., Yiou, P., Haeffelin, M., Dupont, J.-C., Stéfanon,
765 M., 2014. European heatwave in July 2006: Observations and modeling
766 showing how local processes amplify conducive large-scale conditions. Geo-
767 physical Research Letters 41 (15), 5644–5652.

768 Dee, D. P., Uppala, S. M., Simmons, A. J., Berrisford, P., Poli, P., Kobayashi,
769 S., Andrae, U., Balmaseda, M. A., Balsamo, G., Bauer, P., Bechtold, P.,
770 Beljaars, A. C. M., Van De Berg, L., Bidlot, J., Bormann, N., Delsol,
771 C., Dragani, R., Fuentes, M., Geer, A. J., Haimberger, L., Healy, S. B.,
772 Hersbach, H., Hólm, E. V., Isaksen, L., K\a allberg, P., Köhler, M., Ma-
773 tricardi, M., McNally, A. P., Monge-Sanz, B. M., Morcrette, J. J., Park,
774 B. K., Peubey, C., De Rosnay, P., Tavolato, C., Thépaut, J. N., Vitart, F.,
775 2011. The ERA-Interim reanalysis: configuration and performance of the
776 data assimilation system. Q. J. R. Meteorol. Soc. 137 (656), 553–597.

777 Del Río, P., Calvo Silvosa, A., Iglesias Gómez, G., 2011. Policies and de-
778 sign elements for the repowering of wind farms: A qualitative analysis of
779 different options. Energy Policy 39 (4), 1897–1908.

780 Drobinski, P., Anav, A., Lebeaupin Brossier, C., Samson, G., Stéfanon, M.,
781 Bastin, S., Baklouti, M., Béranger, K., Beuvier, J., Bourdallé-Badie, R.,
782 Coquart, L., D'Andrea, F., de Noblet-Ducoudré, N., Diaz, F., Dutay, J.-
783 C., Ethe, C., Foujols, M.-A., Khvorostyanov, D., Madec, G., Mancip, M.,
784 Masson, S., Menut, L., Palmieri, J., Polcher, J., Turquety, S., Valcke,
785 S., Viovy, N., Jul. 2012. Model of the Regional Coupled Earth system
786 (MORCE): Application to process and climate studies in vulnerable re-
787 gions. Environmental Modelling & Software 35, 1–18.

788 Drobinski, P., Ducrocq, V., Alpert, P., Anagnostou, E., Béranger, K.,
789 Borga, M., Braud, I., Chanzy, A., Davolio, S., Delrieu, G., Estournel, C.,
790 Boubrahmi, N. F., Font, J., Grubišić, V., Gualdi, S., Homar, V., Ivančan-
791 Picek, B., Kottmeier, C., Kotroni, V., Lagouvardos, K., Lionello, P.,
792 Llasat, M. C., Ludwig, W., Lutoff, C., Mariotti, A., Richard, E., Romero,
793 R., Rotunno, R., Roussot, O., Ruin, I., Somot, S., Taupier-Letage, I., Tin-
794 tore, J., Uijlenhoet, R., Wernli, H., Jul. 2014. HyMeX A 10-Year Multidis-
795 ciplinary Program on the Mediterranean Water Cycle. Bull. Am. Meteorol.
796 Soc. 95 (7), 1063–1082.

797 Duffie, J., Beckman, W., 2013. Solar Engineering of Thermal Processes, 4th
798 Edition. John Wiley & Sons, Hoboken.

799 Elliston, B., Diesendorf, M., MacGill, I., Jun. 2012. Simulations of scenar-
800 ios with 100% renewable electricity in the Australian National Electricity
801 Market. Energy Policy 45, 606–613.

802 Flaounas, E., Drobinski, P., Vrac, M., Bastin, S., Lebeaupin-Brossier, C.,
803 Stéfanon, M., Borga, M., Calvet, J.-C., Jun. 2013. Precipitation and tem-
804 perature space–time variability and extremes in the Mediterranean region:
805 evaluation of dynamical and statistical downscaling methods. Climate Dy-
806 namics 40 (11-12), 2687–2705.

807 GSE, 2015. Rapporto Statistico 2015: Energia da fonti rinnovabili in Italia.
808 Tech. rep., GSE.

809 GSE, 2016. Rapporto Statistico 2016: Energia da fonti rinnovabili in Italia.
810 Tech. rep., GSE.

811 Hastie, T., Tibshirani, R., Friedman, J., 2009. The Elements of Statistical
812 Learning, 2nd Edition. Springer, New York.

Heide, D., Greiner, M., von Bremen, L., Hoffmann, C., 2011. Reduced storage and balancing needs in a fully renewable European power system with excess wind and solar power generation. Renew. Energy 36 (9), 2515–2523.

Heide, D., von Bremen, L., Greiner, M., Hoffmann, C., Speckmann, M., Bofinger, S., 2010. Seasonal optimal mix of wind and solar power in a future, highly renewable Europe. Renew. Energy 35 (11), 2483–2489.

Hirth, L., 2013. The market value of variable renewables. The effect of solar wind power variability on their relative price. Energy Econ. 38, 218–236.

Hosenuzzaman, M., Rahim, N. A., Selvaraj, J., Hasanuzzaman, M., Malek, A. B. M. A., Nahar, A., Jan. 2015. Global prospects, progress, policies, and environmental impact of solar photovoltaic power generation. Renewable and Sustainable Energy Reviews 41, 284–297.

Huber, M., Dimkova, D., Hamacher, T., 2014. Integration of wind and solar power in Europe: Assessment of flexibility requirements. Energy 69, 236–246.

IEA, 2017. World Energy Outlook 2017. Tech. rep., IEA.

Justus, C. G., Mikhail, A., 1976. Height variation of wind speed and wind distributions statistics. Geophysical Research Letters 3 (5), 261–264.

Lebeaupin Brossier, C. L., Bastin, S., Béranger, K., Drobinski, P., Feb. 2015. Regional mesoscale air–sea coupling impacts and extreme meteorological events role on the Mediterranean Sea water budget. Climate Dynamics 44 (3-4), 1029–1051.

Lebeaupin Brossier, C. L., Drobinski, P., Béranger, K., Bastin, S., Orain, F., 2013. Ocean memory effect on the dynamics of coastal heavy precipitation preceded by a mistral event in the northwestern Mediterranean. Quarterly Journal of the Royal Meteorological Society 139 (675), 1583–1597.

Lund, H., Mathiesen, B. V., 2009. Energy system analysis of 100% renewable energy systems-The case of Denmark in years 2030 and 2050. Energy 34 (5), 524–531.

MacKay, D. J. C., 1992. Bayesian Interpolation. Neural Computation 4 (3), 415–447.

Mencarelli, L., D'Ambrosio, C., 2018. Complex portfolio selection via convex mixed-integer quadratic programming: a survey. International Transactions in Operational Research.

Miettinen, K. M., 1999. Nonlinear Multiobjective Optimization. Springer, New York.

Nelson, J., Johnston, J., Mileva, A., Fripp, M., Hoffman, I., Petros-Good, A., Blanco, C., Kammen, D. M., 2012. High-resolution modeling of the western North American power system demonstrates low-cost and low-carbon futures. Energy Policy 43, 436–447.

Omrani, H., Drobinski, P., Arsouze, T., Bastin, S., Lebeaupin-Brossier, C., Mailler, S., Feb. 2017. Spatial and temporal variability of wind energy resource and production over the North Western Mediterranean Sea: Sensitivity to air-sea interactions. Renewable Energy 101, 680–689.

Omrani, H., Drobinski, P., Dubos, T., Nov. 2013. Optimal nudging strategies in regional climate modelling: investigation in a Big-Brother experiment over the European and Mediterranean regions. Climate Dynamics 41 (9-10), 2451–2470.

Omrani, H., Drobinski, P., Dubos, T., Mar. 2015. Using nudging to improve global-regional dynamic consistency in limited-area climate modeling: What should we nudge? Climate Dynamics 44 (5-6), 1627–1644.

Reindl, D. T., Beckman, W. A., Duffie, J. A., Jan. 1990a. Diffuse fraction correlations. Solar Energy 45 (1), 1–7.

Reindl, D. T., Beckman, W. A., Duffie, J. A., Jan. 1990b. Evaluation of hourly tilted surface radiation models. Solar Energy 45 (1), 9–17.

Rodríguez, R. A., Becker, S., Andresen, G. B., Heide, D., Greiner, M., 2014. Transmission needs across a fully renewable European power system. Renew. Energy 63, 467–476.

Roques, F., Hiroux, C., Saguan, M., 2010. Optimal wind power deployment in Europe-A portfolio approach. Energy Policy 38 (7), 3245–3256.

Ruti, P. M., Somot, S., Giorgi, F., Dubois, C., Flaounas, E., Obermann, A., Dell'Aquila, A., Pisacane, G., Harzallah, A., Lombardi, E., Ahrens, B.,

Akhtar, N., Alias, A., Arsouze, T., Aznar, R., Bastin, S., Bartholy, J., Béranger, K., Beuvier, J., Bouffies-Cloché, S., Brauch, J., Cabos, W., Calmanti, S., Calvet, J. C., Carillo, A., Conte, D., Coppola, E., Djurdjevic, V., Drobinski, P., Elizalde-Arellano, A., Gaertner, M., Galàn, P., Gallardo, C., Gualdi, S., Goncalves, M., Jorba, O., Jordà, G., L'Heveder, B., Lebeaupin-Brossier, C., Li, L., Liguori, G., Lionello, P., Maciàs, D., Nabat, P., Önol, B., Raikovic, B., Ramage, K., Sevault, F., Sannino, G., Struglia, M. V., Sanna, A., Torma, C., Vervatis, V., 2016. Med-CORDEX initiative for Mediterranean climate studies. Bull. Am. Meteorol. Soc. 97 (7), 1187–1208.

Salameh, T., Drobinski, P., Dubos, T., 2010. The effect of indiscriminate nudging time on large and small scales in regional climate modelling: Application to the Mediterranean basin. Quarterly Journal of the Royal Meteorological Society 136 (646), 170–182.

Santos-Alamillos, F. J., Thomaidis, N. S., Usaola-García, J., Ruiz-Arias, J. A., Pozo-Vázquez, D., 2017. Exploring the mean-variance portfolio optimization approach for planning wind repowering actions in Spain. Renew. Energy 106, 335–342.

Skamarock, W. C., Klemp, J. B., Dudhia, J., Gill, D. O., Barker, D. M., Wang, W., Powers, J. G., Jun. 2005. A Description of the Advanced Research WRF Version 2. Tech. Rep. NCAR/TN-468+STR, NATIONAL CENTER FOR ATMOSPHERIC RESEARCH BOULDER CO MESOSCALE AND MICROSCALE METEOROLOGY DIV, NATIONAL CENTER FOR ATMOSPHERIC RESEARCH BOULDER CO MESOSCALE AND MICROSCALE METEOROLOGY DIV.

Skoplaki, E., Palyvos, J. A., May 2009. On the temperature dependence of photovoltaic module electrical performance: A review of efficiency/power correlations. Solar Energy 83 (5), 614–624.

Spiecker, S., Weber, C., 2014. The future of the european electricity system and the impact of fluctuating renewable energy - A scenario analysis. Energy Policy 65, 185–197.

Stéfanon, M., Drobinski, P., D'Andrea, F., Lebeaupin-Brossier, C., Bastin, S., Mar. 2014. Soil moisture-temperature feedbacks at meso-scale during

summer heat waves over Western Europe. Climate Dynamics 42 (5-6), 1309–1324.

Terna, 2016. Sustainability Report 2016. Tech. rep., Terna, Rome.

Thomaidis, N. S., Santos-Alamillos, F. J., Pozo-Vázquez, D., Usaola-García, J., 2016. Optimal management of wind and solar energy resources. Comput. Oper. Res. 66, 284–291.

Tsuchiya, H., 2012. Electricity supply largely from solar and wind resources in Japan. Renew. Energy 48, 318–325.

Widén, J., 2011. Correlations between large-scale solar and wind power in a future scenario for Sweden. IEEE Trans. Sustain. Energy 2 (2), 177–184.

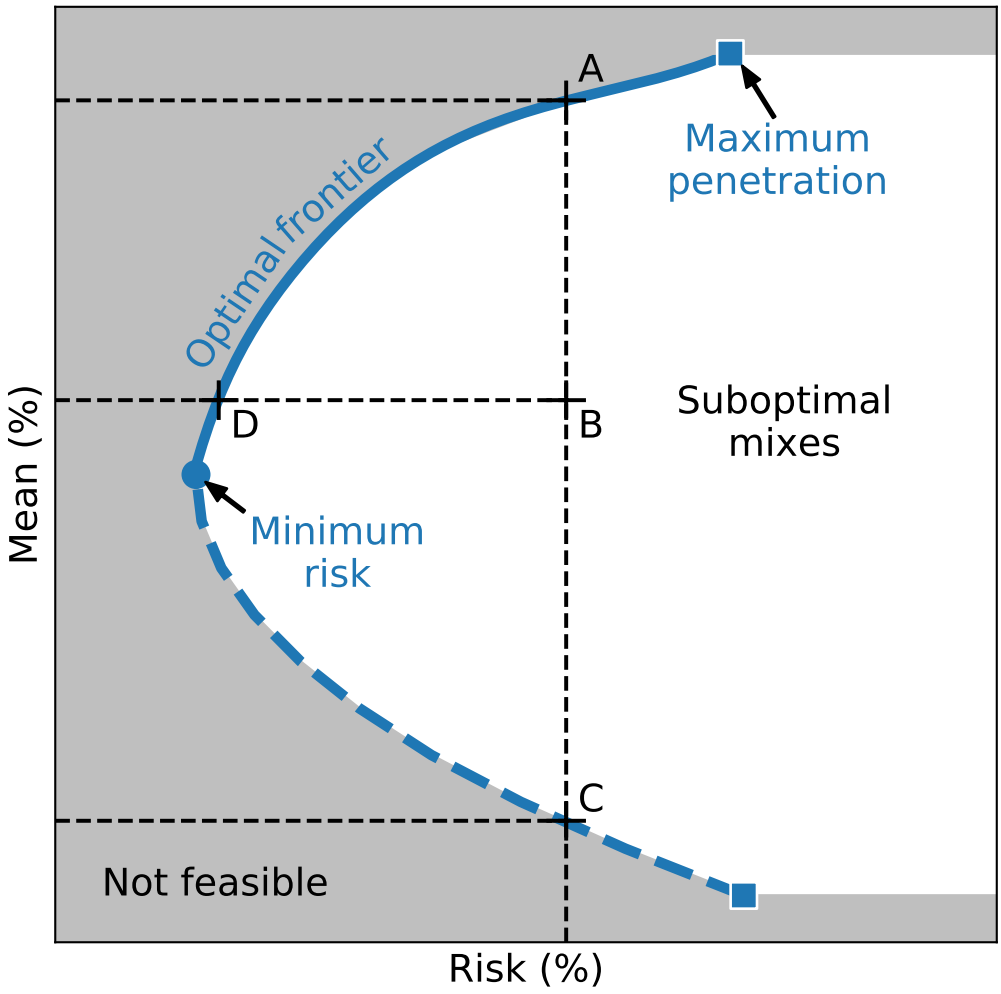

Figure 7: Example of the optimal frontier of a mean-variance bi-objective optimization problem. The optimal frontier is one-dimensional and represented by a plain blue line. Mixes in the white region to the right of the frontier are suboptimal. Points in the gray region to the left of the frontier are not feasible. In this example, the optimal frontier is bounded below by a minimum-risk optimal-mix (blue dot) below which the risk may only increase. The optimal frontier is bounded above by a maximum-penetration optimal-mix above which higher penetration mixes are not feasible due to the constraints of the problem. The point B is an example of suboptimal mix, since a higher mean penetration is achievable for the same risk (point A) and a lower risk is achievable for the same mean penetration (point D). The dashed blue line is obtained by minimizing the risk for a range of target mean penetration values. These solutions are, however, not Pareto optimal. For instance, point C yields the same risk as point A but achieves a lower mean penetration. Thus, A "dominates" C.

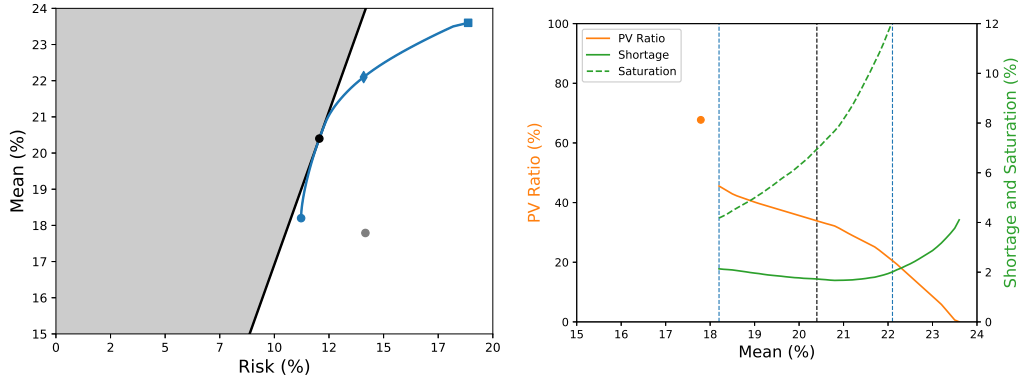

(a) $\alpha_{\text{global}} = 1.69$ (b)

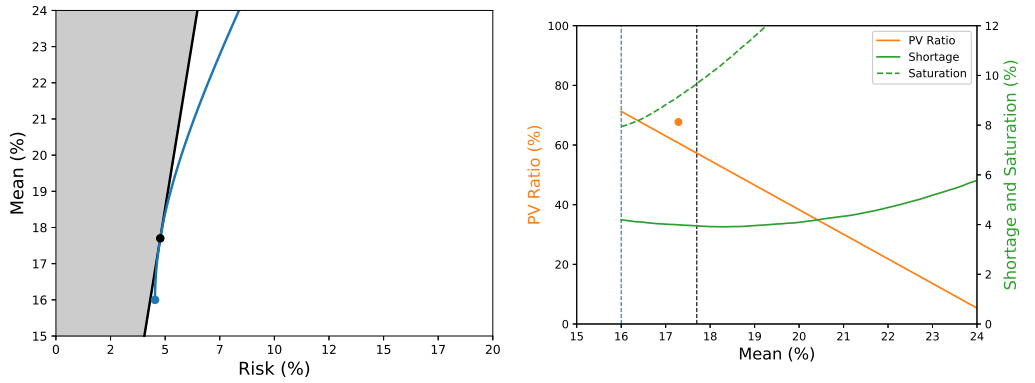

(c) $\alpha_{\text{regional}} = 3.71$ (d)

Figure 8: Approximations of the optimal frontiers (left) and of the corresponding electricity mix characteristics (right) for the global (top) and the regional (bottom) optimization problems. The blue curve in the left panels represents the approximation of the optimal frontier of the optimization problem (10). The straight black line is the optimal frontier of the same problem, but with the total capacity constraint (10c) removed. The approximations were obtained using a discretization step of 0.1%. The black dot where the black frontier is tangent to the blue one corresponds to the optimal electricity mix for which the total capacity constraint is inactive (i.e. where adding this constraint has no effect on the results of the optimization problem). The blue dots in panels (a) and (c) correspond to the optimal energy mix for which the risk is minimized while satisfying the total capacity constraint. The gray dot in panel (a) is obtained from the same capacity factor and demand data but applying the actual capacities installed in Italy in 2015 (cf. Tab. 2). The blue diamond corresponds to the optimal mix achieving the same level of risk as the actual mix in gray while maximizing the mean penetration. The blue squares correspond to limits beyond which it is not possible to further decrease or increase the mean total penetration while satisfying the total capacity constraint and the bounds. The values of the mean-risk ratio of the unconstrained optimal frontiers, given by (11), are also reported in the sub-captions. On the right panels are represented the fraction of photovoltaic capacity in the mix (plain orange line), or PV ratio as well as the shortage (plain green line) and saturation (dashed green line) frequencies versus the mean penetration. The blue and black dashed vertical lines mark the mean penetration values corresponding to the blue and black dots and the blue diamond on the left panels. The orange dot represents the PV ratio for the actual capacities installed in Italy in 2015.

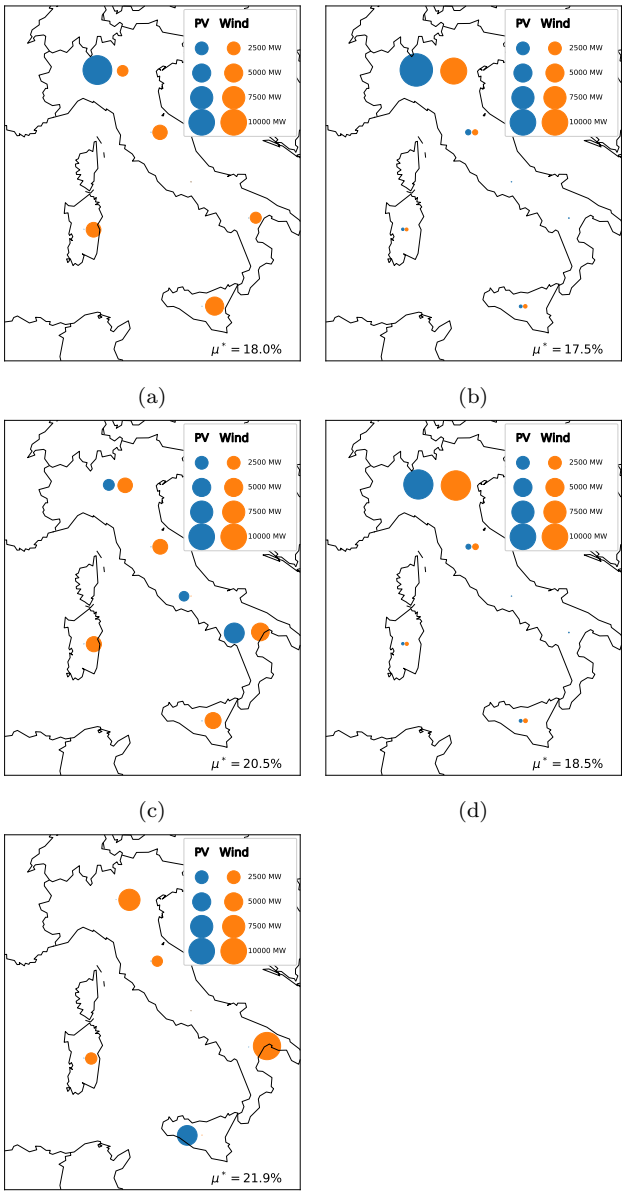

Figure 9: Geographical and technological distribution of the RES capacity for the global (left) and regional (right) optimal mixes respecting the total capacity constraint. The top, middle and bottom panels represent the optimal mixes for the minimum risk, maximum mean-risk ratio and higher penetration scenarios, respectively (blue dot, black dot and blue diamond in Fig. 8a and 8c). Note that there is no plot of the higher penetration scenario for the regional strategy since the regional risk of the actual mix is too high to be achieved by an optimal mix.

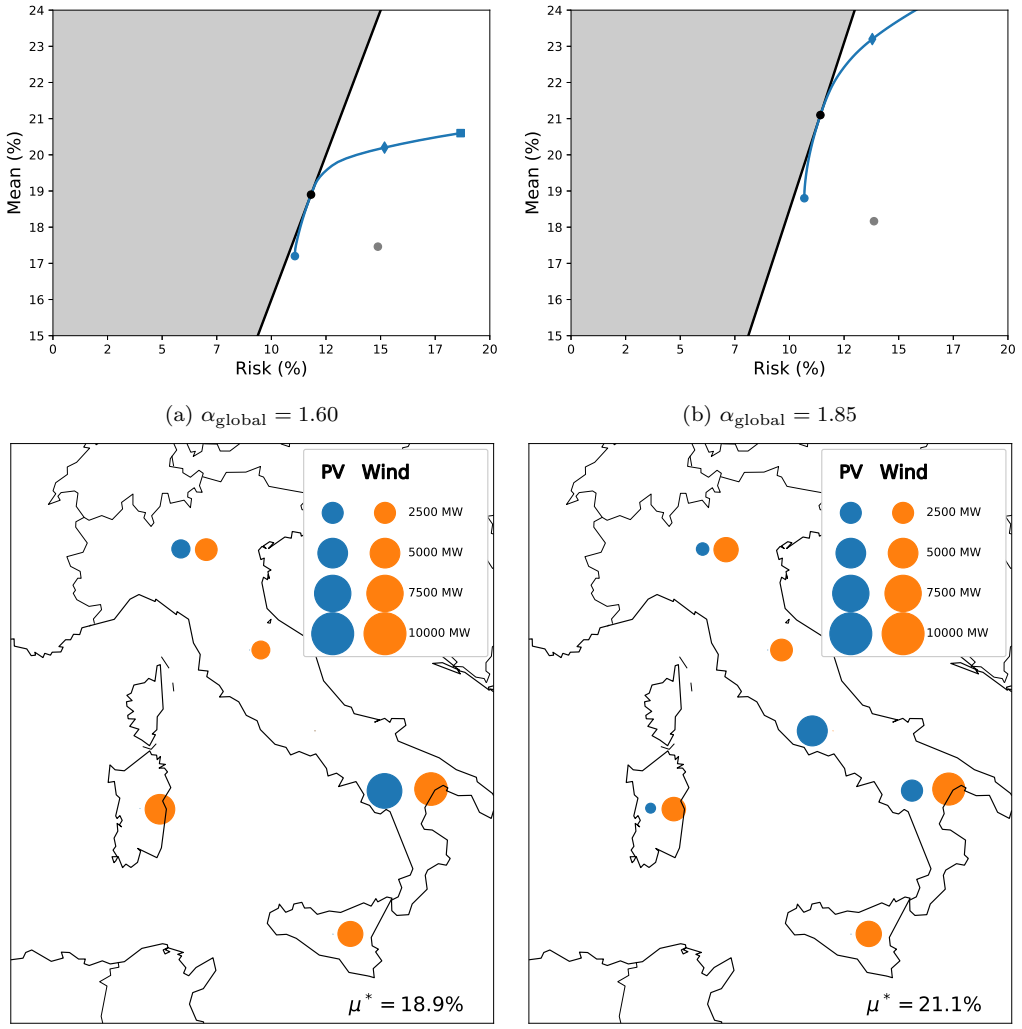

(a) $\alpha_{\text{global}} = 1.60$

(b) $\alpha_{\text{global}} = 1.85$

(c) 1989

(d) 1996

Figure 10: Approximated Pareto frontiers (top) and geographical and technological distribution of the RES capacity (bottom) for the global optimization problem solved for the years 1989 (left) and 1996 (right). The approximations were obtained using a discretization step of 0.1%. The legend is the same as for Fig. 8 and Fig. 9.

.